IEEE Access
Multidisciplinary | Rapid Review | Open Access Journal

Received 14 July 2022, accepted 29 July 2022, date of publication 8 August 2022, date of current version 16 August 2022.

Digital Object Identifier 10.1109/ACCESS.2022.3197604

RESEARCH ARTICLE

Modeling and Simulation of a Packed Column Batch Still for Fruit Wine Distillations

SIMÓN DÍAZ-QUEZADA[1], DAVID I. WILSON[2], AND JOSÉ R. PÉREZ-CORREA[1]
[1]Chemical and Bioprocess Engineering Department, Pontificia Universidad Católica de Chile, Santiago 7820436, Chile
[2]Industrial Information Control Centre, Auckland University of Technology, Auckland 1023, New Zealand

Corresponding author: José R. Pérez-Correa (perez@ing.puc.cl)

The work of Simón Díaz-Quezada was supported in part by the Vicerrectoria de Investigación de la Pontificia Universidad Católica de Chile through a scholarship, and in part by an Internship at the Auckland University of Technology.

ABSTRACT Batch distillations are extensively used worldwide to produce fruit wine spirits with distinctive aromas. These processes are typically operated manually, based on the experience of the distiller. However, dynamic optimization and automatic control strategies could be valuable for ensuring a more consistent product and quickly adapting to new market tendencies. Consequently, reliable process models are required for the application of these methods. The novelty of this study is developing a highly efficient method to reliably simulate and calibrate a rigorous first-principles model of a packed batch column still. We applied the method of lines (MOL) to transform the partial differential equations describing the packed column dynamics into an ordinary differential equation (ODE) system. The nonlinear phase equilibrium equations were presolved, and several polynomials were fitted to get explicit algebraic equations. The final differential-algebraic system (DAE) comprises 31 ODEs, 113 explicit algebraic equations, and two implicit algebraic equations. Variables scaling, smoothing of discontinuities, and applying an algebraic loop within Simulink to solve the implicit algebraic equations resulted in 600 times faster simulations than a naïve approach. The model was regressed using pilot-scale experimental data and subjected to extensive validation using independent data. Sensitivity and residual analysis established that a better heat loss model could improve ethanol concentration prediction. This new heat loss model reduced the average ethanol concentration error by more than five times. The developed model can be applied to design reliable control systems and optimal operating strategies for packed column batch distillations.

INDEX TERMS Differential algebraic systems, model calibration, algebraic loops, first-principles models.

I. INTRODUCTION

Since ancient times in China, Mediterranean cultures, and worldwide, skilled distillers have produced distilled spirits using various fermented fruits and grains [1]. These define the specific spirit; for instance, whiskey is produced from barley (the UK and Ireland), cachaça from sugar cane (Brazil), tequila from agave (Mexico), and cognac, brandy, and pisco from grapes (France, Spain, Chile, and Peru). A specific set of trace compounds of these distillates, primarily terpenes and esters, gives them distinctive aromatic characteristics [2], [3], [4], [5], [6], [7]. Nevertheless, distilled spirits also contain undesirable (fatty acids and higher alcohols) and toxic compounds (methanol, acetaldehyde, and furfural), which Law generally limits. Aromatic, undesirable, and toxic compounds are minor components in distillates and are usually called congeners. These come from the fruit or grain, generated during fermentation or incorporated during aging, and a fraction is recovered during distillation. Hence, the final aromatic characteristic of the distillate depends not only on the fruit or grain quality but also on the process operation during fermentation, distillation, and aging [8], [9], [10], [11], [12], [13], [14]. Specifically, the process operator defines the distillation time and operating conditions to achieve the desired product.

Batch distillation is crucial to producing high-quality distilled spirits because the desired aromas can be selectively recovered by adequately managing the cuts (head, heart,

The associate editor coordinating the review of this manuscript and approving it for publication was Mauro Gaggero.

and tail) and the operating variables (reboiler heating and reflux rate). The available operation flexibility depends on the equipment: alembics (lower) and column stills (higher). Copper alembics have been traditionally used for hundreds of years to produce spirits, and their operation has been thoroughly studied [15], [16], [17], [18]. Alembics take advantage of the ambient temperature to produce natural reflux while the operator manages the reboiler heating. Spirits batch distillations can also be carried out in batch column stills using either packed bed or plate rectification columns. This system allows for a more flexible operation than alembics because the operator can manage the reflux rate through the coolant flow rate in the partial condenser [19], [20], [21], [22], [23], [24]. Nevertheless, batch column stills are subjected to more uncontrolled disturbances and manipulable variables, such as temperature and inlet flow coolant, resulting in a much less reproducible operation than alembics [7], [25].

Dynamic mathematical models help control and optimize the operation of alembics and batch column stills. However, similar to most chemical processing plants, developing models for complex unit operations is challenging because of their nonlinear behavior, varying dynamics, unmeasured disturbances, discontinuous functions, and spatial and temporal variation [1], [26], [27], [28], [29], [30], [31], [32]. Of direct relevance to this study, some first-principles mathematical models have been developed for spirits batch distillations in packed columns [21], [33], as well as for other distillation systems as trays columns [34], [35], and copper alembics [36], [37], [38], [39], [40].

State of the art suggests that modeling, simulation, and calibration of packed column batch stills for fruit wine distillations is a challenge not satisfactorily solved yet. The additional complexity of modeling packed column stills, compared to other spirits batch processes, is that partial differential equations (PDE) are required to describe the column dynamics fully. Previous modeling efforts could not adequately reproduce the experimentally observed dynamics, and simulations were slow [21], [30], [33]. The thermal inertia of the column wall and heat losses were not considered in these models, and the chosen strategy for numerically solving the PDE system was computationally demanding. The latter inefficiency is due to the complexity of numerically solving partial differential-algebraic equation (PDAE) systems [41], [42], [43], [44]. Slow simulations impair reliable model calibrations, process optimization, and process control design because they typically require thousands of simulations to yield adequate results.

The model for fruit wine batch distillations in packed columns developed in this study contributes to the next key points:

- An improved description of its thermal behavior through a detailed heat transfer model in the partial condenser.
- The addition of the thermal inertia of the packed column in the dynamic energy balances and the explicit consideration of heat losses in both the partial condenser and packed column.
- A more efficient numerical method by applying ''algebraic loops'' in Simulink or explicitly employing a left-hand side mass matrix for the ODE solver ODE15s in MATLAB depending on the DAE index [45], [46].
- The discontinuous model functions (e.g., laminar/turbulent regime flow correlation) were approximated by smooth transition functions, and model variables were scaled [47].

The model developed in this study cannot be compared with current fruit distillation models due to differences in key phenomenological aspects. For instance, in alembics, the reflux rate is not controllable since it is defined by the heat transfer to the environment due to natural convection [37], [38], [39], [40], [48]. In turn, in batch distillation columns, the reflux rate is defined by the heat transfer to the flowing cooling water; hence, the reflux rate can be controlled by changing the water flow rate. In addition, alternative batch column models for fruit wine distillations are substantially different since they consider plate columns instead of packed columns or do not include heat accumulation and heat loss in the rectification column [21], [34].

The remainder of this paper is organized as follows: Section II describes the pilot-scale packed distillation column, the resultant model, and the numerical strategy applied to solve it; Section III describes the results and comments on the general model behavior, model calibration, validation results, and sensitivity analysis; finally, the main findings of this research are summarized in the conclusion section.

II. METHODOLOGY

A. THE BATCH DISTILLATION COLUMN

We modeled the pilot-scale packed column at the Chemical and Bioprocess Engineering Department at the *Pontificia Universidad Católica de Chile,* as shown in Fig. 1. This fully automatic distiller, made of stainless steel, is composed of: i) a 50 L reboiler; ii) a 28 cm high x 5 cm diameter column filled with 5 mm glass Raschig rings; iii) an internal partial condenser above the column with 160 cm^2 coil external surface; iv) a total condenser on the top of the column with a 500 cm^2 contact area to ensure a complete condensation of the distillate. The entire distiller was thermally insulated with 10 mm thick elastomeric rubber foam to minimize heat losses.

The batch still instrumentation includes (Fig.1): i) two AC phase controllers using TRIAC for the variable electric power on the immersion heaters (0-2000 W) in the reboiler; ii) a variable flow cooling water peristaltic pump (0-300 mL/min) for the partial condenser; iii) eight PT-100 temperature sensors distributed in the distiller; iv) a density sensor (Anton-Paar, L-Dens 2300) to measure the ethanol concentration in the distillate; v) two flowmeters, one for the distillate, and the other for the partial condenser cooling water. Further instrumentation details of this still are given in [30].

B. BATCH DISTILLATION OPERATION

The distillation process begins by heating the liquid mixture loaded into the reboiler until the distillate production begins.

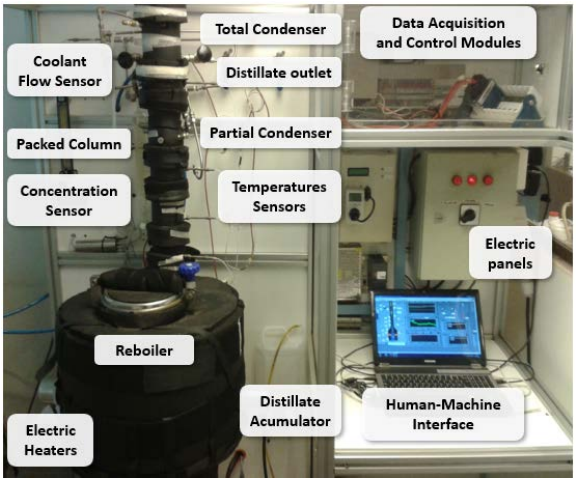

FIGURE 1. The batch distillation column still used in the experiments.

The initial feed mixture contained 13% v/v ethanol and 1.5 g methanol/L of pure ethanol (p.a.). Initially, the reboiler heating power, Q_b, was set to 1000 W, the cooling water flow rate at the partial condenser, F_w, is set to 150 mL/min, and the inlet cooling water temperature, $T_{w,in}$, was 20 °C. The total condenser cooling stream (kept over 5000 mL/min) is impulsed directly from the tap water obtained in the laboratory.

Like wine distillate industries, the distillate is separated into three "cuts," where a specific time indicates when the transition occurs. The first cut is the head, associated with the initial distillate, which is rich in low-quality aromatic components; the cut time of this stage ranges from 3 to 10 min after the heating start-up time (1 h at 1000 W). The second cut was the heart, the primary and most extended distillation stage (up to 5 h). Our simulations focus on the heart cut since process optimization and control are essential in this stage to achieve a good quality product. The third cut is the tail, rich in undesirable aromas like fatty acids. Typically, the head and tail cuts are mixed and redistilled to recover more ethanol.

C. DISTILLATION MODEL

The model developed here extends the non-equilibrium model proposed in [21]. The following main assumptions were considered to balance model accuracy and numerical efficiency:

i) The ternary mixture comprises ethanol and water as the main components, and methanol, which is a toxic congener.
ii) The reboiler and partial condenser are perfectly mixed.
iii) The vapor/liquid equilibrium (VLE) of water and ethanol and the physical and transport properties of the mixtures are not affected by methanol.
iv) The vapor phase is considered an ideal gas in thermodynamic equilibrium.
v) Equimolar distillation is assumed due to the minor differences between the latent heats.
vi) No vapor accumulation in the system is considered (the vapor phase is in a pseudo-steady-state).
vii) The packed column presents local thermal equilibrium.
viii) Radial temperature and concentration gradients are negligible; only longitudinal variations are considered.
ix) The reboiler and partial condenser are considered in thermodynamic equilibrium.

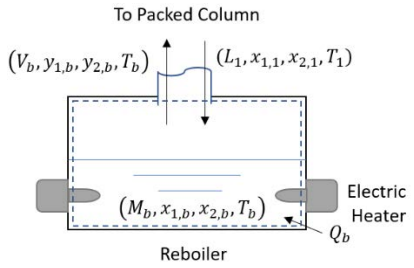

FIGURE 2. Control volume diagram of the reboiler.

1) MASS AND ENERGY BALANCES: REBOILER

The dynamic balances (Fig. 2) for the reboiler are described by *ordinary* differential equations (ODE) given assumption (ii). The total mass balance of the liquid phase (1) includes the liquid molar flow rate L_1, coming down from the packed column, and the vapor molar flow rate V_b, produced by the reboiler heaters. The ethanol (2) and methanol (3) liquid mass balances consider the corresponding liquid ($x_{1,1}$, $x_{2,1}$) and vapor ($y_{1,b}$, $y_{2,b}$) molar fractions, respectively. The energy balance (4) is expressed in terms of the liquid, h_1, and vapor, H_b, stream enthalpies and the power supplied by the reboiler heaters, Q_b. The reboiler heat losses were typically small because it is thermally insulated and electrically heated.

$$\frac{dM_b}{dt} = L_1 - V_b \tag{1}$$

$$\frac{d\left(M_b x_{1,b}\right)}{dt} = L_1 x_{1,1} - V_b y_{1,b} \tag{2}$$

$$\frac{d\left(M_b x_{2,b}\right)}{dt} = L_1 x_{2,1} - V_b y_{2,b} \tag{3}$$

$$\frac{d\left(M_b h_b\right)}{dt} = L_1 h_1 - V_b H_b + Q_b \tag{4}$$

2) MASS AND ENERGY BALANCES: PACKED COLUMN

It is necessary to employ PDEs to describe the mass and energy balances in the packed column section (Fig. 3) because the temperature and concentrations depend on the time and longitudinal position (assumption viii).

The total mass balance (5) includes the accumulation of liquid holdup in the packing section, M', and the difference between the liquid flow rate, L, and the vapor flow rate, V. Furthermore, the mass balances for ethanol (6) and methanol (7) also consider their liquid (x_1, x_2) and vapor (y_1, y_2) molar fractions. The energy balance (8) includes the enthalpies of the liquid, h, and vapor, H, streams, and the heat loss, Q'_{loss}, through the column wall, assumed to be independent of time and height. The accumulation term in the energy

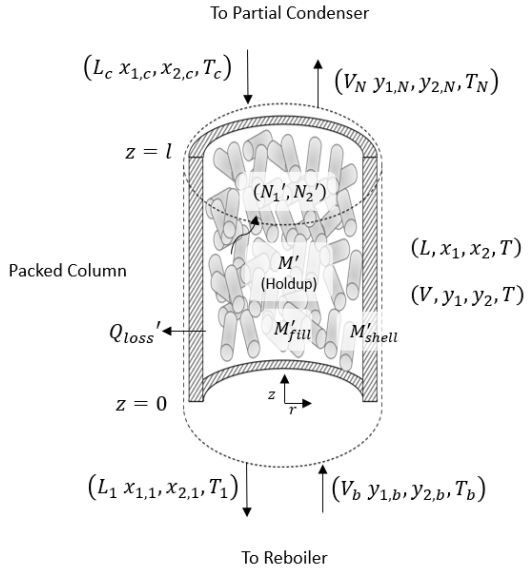

FIGURE 3. Control volume diagram of the packed column.

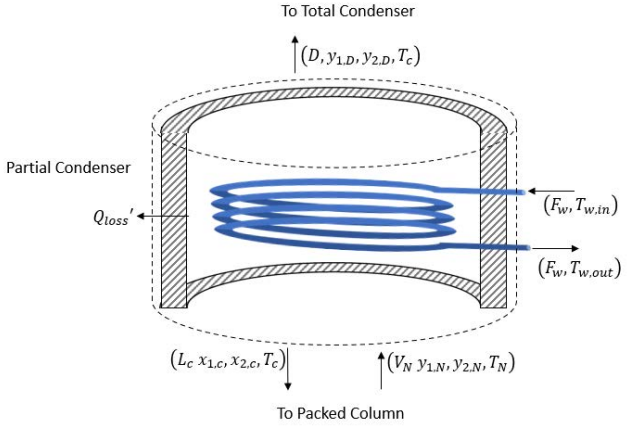

FIGURE 4. Control volume diagram of the partial condenser.

balance includes three contributions: liquid holdup, column wall, and packing itself. According to assumption (vii), the packing, column metal wall, and liquid holdup are at the same temperature. Q'_{loss} and $M'_{shell}Cp_{shell}$ are considered free parameters to be regressed in this model. Because vapor accumulation is negligible (assumption vi), the vapor phase mass balances for ethanol (9) and methanol (10) do not include the time-derivative term. These equations include the phase vapor/liquid mass transfer flux for ethanol and methanol (N'_1, N'_2), associated with the cross-section area, S.

$$\frac{dM'}{dt} = \frac{\partial L}{\partial z} - \frac{\partial V}{\partial z} \tag{5}$$

$$\frac{d(M'x_1)}{dt} = \frac{\partial (Lx_1)}{\partial z} - \frac{\partial (Vy_1)}{\partial z} \tag{6}$$

$$\frac{d(M'x_2)}{dt} = \frac{\partial (Lx_2)}{\partial z} - \frac{\partial (Vy_2)}{\partial z} \tag{7}$$

$$\frac{d\left(M'h + M'_{shell}Cp_{shell}T + M'_{fill}Cp_{fill}T\right)}{dt} = \cdots \frac{\partial (Lh)}{\partial z} - \frac{\partial\,(VH)}{\partial z} - Q'_{loss} \tag{8}$$

$$0 = -\frac{\partial\,(Vy_1)}{\partial z} + SN'_1 \tag{9}$$

$$0 = -\frac{\partial\,(Vy_2)}{\partial z} + SN'_2 \tag{10}$$

3) MASS AND ENERGY BALANCES: PARTIAL CONDENSER

Part of the vapor coming from the packed column condensate over the cooling-coil surface of the partial condenser (Fig. 4). This stage is considered in thermodynamic equilibrium and pseudo-steady-state (fast dynamics, small holdup); hence, the energy and mass balances are represented by algebraic equations only.

The total mass balance (11) includes the molar flow rate of the outlet vapor that condenses in the total condenser (distillate D), the flow rate of the vapor coming from the column, V_n, and the flow rate of the condensed liquid that is returned to the column (reflux L_c). The respective mass balances for ethanol (12) and methanol (13) also include the corresponding molar fraction of each stream. Energy balance (14) considers the heat removed by the cooling water, Q_C, and the enthalpies of the corresponding inlet and outlet streams. The removed heat in the form of sensible heat is given by (15). In the next section, that heat is constrained by (22).

$$0 = V_n - L_c - D \tag{11}$$

$$0 = V_n y_{1,n} - L_c x_{1,c} - D y_{1,d} \tag{12}$$

$$0 = V_n y_{2,n} - L_c x_{2,c} - D y_{2,d} \tag{13}$$

$$0 = V_n H_n - L_c h_c - D H_d - Q_C \tag{14}$$

$$Q_C = F_w \rho_w c_{p,w} \left(T_{w,out} - T_{w,in}\right) \tag{15}$$

4) CONSTITUTIVE EQUATIONS

Additional relationships are required from the established mass and energy balances. These algebraic equations represent this system's transport phenomena mechanisms, vapor/liquid equilibrium, and physical properties. Specifically, in this model, the constitutive equations include: i) mass transfer and hydraulics in the packed column, ii) vapor/liquid thermodynamic equilibrium models, iii) heat transfer correlations in the partial condenser, and iv) physical properties of the liquid and vapor mixtures (density, viscosity, surface tension, thermal conductivity, heat capacity, and enthalpies) as a function of temperature and composition.

a: MASS TRANSFER IN THE PACKED COLUMN

An equimolar distillation model is applied (assumption v), meaning that the molar flow rates of each component between the liquid and vapor phases are given by the Maxwell-Stefan double resistance model for multicomponent transport [49],

which is determined by the resistance between the interface (describing phase equilibrium with superscript $*$) and the bulk of the liquid phase. The molar transfer rates depending on the packing height are given for ethanol:

$$N_1' = k_{13}a_{e_{13}}\rho\left(x_1^* - x_1\right) \tag{16}$$

and methanol,

$$N_2' = \left(\frac{x_1}{k_{21}a_{e_{21}}} + \frac{1-x_1}{k_{23}a_{e_{23}}}\right)^{-1}\rho\left(x_2^* - x_2\right) \tag{17}$$

These include the volumetric mass transfer coefficients of the binary pairs (ethanol-water, $k_{13}a_{e_{13}}$; methanol-ethanol, $k_{21}a_{e_{21}}$; and methanol-water, $k_{23}a_{e_{23}}$). The ethanol molar transfer rate does not depend on the methanol concentration because the latter is very small compared with the ethanol and water concentrations.

The mass transfer correlations for packed columns,

$$k_{ij} = C_M\left(\frac{\rho g}{\mu}\right)^{\frac{1}{6}}\left(\frac{D_{ij}}{l_{eq}}\right)^{\frac{1}{2}}\left(\frac{LMW_{ij}}{\rho a\phi_{mass}S}\right)^{\frac{1}{3}} \tag{18}$$

$$a_{e_{ij}} = 1.5a\phi_{mass}\left(a\phi_{mass}l_{eq}\right)^{\frac{-1}{2}}\ldots \times\left(\frac{LMW_{ij}l_{eq}}{S\mu}\right)^{\frac{-1}{8}}\left(\frac{L^2MW_{ij}^2}{\rho^2S^2gl_{eq}}\right)^{\frac{-9}{20}}\left(\frac{L^2MW_{ij}^2l_{eq}}{\rho S^2\sigma}\right)^{\frac{3}{4}} \tag{19}$$

were taken from [42].

The main parameter related to mass transfer is the specific interfacial area ($a = 771\ \mathrm{m}^2/\mathrm{m}^3$); this must be multiplied by the effectiveness factor of the mass transfer area, ϕ_{mass} (initially set at 0.83), to obtain the effective area. The latter is estimated from the experimental data, as discussed in Section III. Other mass transfer parameters are the packing constant ($C_M = 1.130$ for glass Raschig rings), and the transversal section area, S, associated with the internal column diameter (52 mm).

b: HEAT TRANSFER IN THE PARTIAL CONDENSER

In the partial condenser, the removed heat, Q_C, is the enthalpy difference between the inlet and outlet streams of the cooling water (15). The heat transfer correlation for laminar/forced flow through pipes [50] defines the heat exchange between the condensing vapor and the cooling water; in this case, the Nusselt number given by

$$Nu_w = \begin{cases} 3.66 & Re_w < 10000 \wedge Gz_w < 2 \\ 1.86Gz_w & Re_w < 10000 \wedge Gz_w \geq 2 \\ 0.027Re_w^{0.8}Pr_w^{\frac{1}{3}}\left(\dfrac{\mu_w}{\mu_w\left(T_c\right)}\right)^{0.14} & Re_w \geq 10000 \end{cases} \tag{20}$$

defines the forced convection on the water side of the coil,

$$h_w = \frac{\lambda_w Nu_w}{d_i} \tag{21}$$

In addition, the thermal resistances due to conduction through the condenser wall and condensation in the vapor side were neglected. The vapor side temperature, T_c, corresponds to the vapor/liquid equilibrium.

TABLE 1. NTRL model parameters.

Parameter	Value	Parameter	Value
τ_{12}	0.2686	G_{12}	0.02519
τ_{21}	−0.0041	G_{21}	1.05791
τ_{13}	−0.0304	G_{13}	1.01118
τ_{31}	1.7292	G_{31}	0.53115
τ_{32}	1.8754	G_{32}	0.77038

For model calibration, this area is multiplied by an effectiveness factor, ϕ_{heat}, which accounts for the unmodelled phenomena.

The algebraic heat transfer model is

$$Q_C = h_w A_c \phi_{heat}\Delta T_{lm} \tag{22}$$

$$\Delta T_{lm} = \frac{T_{w,out} - T_{w,in}}{\ln\left(\frac{T_c - T_{w,in}}{T_c - T_{w,out}}\right)} \tag{23}$$

where the subscript "w" refers to the cooling water. Physical properties, such as viscosity, thermal conductivity, and Prandtl number, were evaluated at the mean temperature $\left(T_{w,out} + T_{w,in}\right)/2$. The Reynolds ($Re$) and Graetz ($Gz$) numbers are required for the appropriate correlation for the Nusselt number (20).

$$Re_w = \frac{\rho_w v d_i}{\mu_w} \tag{24}$$

$$Gz_w = \left(\frac{Re_w Pr_w}{\left(\frac{l}{d_i}\right)}\right)^{\frac{1}{3}}\left(\frac{\mu_w}{\mu_w\left(T_c\right)}\right)^{0.14} \tag{25}$$

c: PACKED COLUMN HYDRAULICS

The liquid velocity down the column, u_L, is given by the packing hydraulics. Reference [51] recommends a correlation for packed beds:

$$u_L = \left(\frac{h_L^3 g^{1.2}\rho^{0.7}}{12C_h^2 a_{ef}^{1.9}\mu^{0.7}}\right)^{\frac{1}{1.7}} \tag{26}$$

which depends on the bulk liquid properties (density and viscosity), effective interfacial area of the packing, a_{ef}, and hydraulic load,h_L. The hydraulic load depends on the liquid holdup, M' (27).

This model is useful for estimating the liquid molar flow rate, L, using (28). Given that the internal diameter of the packed column is $D_s = 5$ cm; hence, the transversal flow section of the column is $S = \pi D_s^2$.

$$h_L = \frac{M'MW}{S\rho} \tag{27}$$

$$L = \frac{u_L\rho S}{MW} \tag{28}$$

d: VAPOR-LIQUID EQUILIBRIUM (ETHANOL-WATER)

The thermodynamic equilibrium is obtained by solving a set of five algebraic equations simultaneously:

Dalton's Law,

$$P_1^0 \gamma_1 x_1 + P_3^0 \gamma_3 (1 - x_1) = P \tag{29}$$

Extended Raoult's Law,

$$P_1^0 \gamma_1 x_1 = P y_1 \tag{30}$$

NTRL activity model (coefficients from [21] are listed in Table 1) for ethanol and water,

$$\begin{aligned} &\ln(\gamma_1) \\ &= \frac{\tau_{31} G_{31} (1 - x_1)}{x_1 + G_{31} (1 - x_1)} \\ &\quad + \ldots \frac{x_1}{x_1 + (1 - x_1) G_{31}} \left(- \left(\frac{(1 - x_1) t31 g31}{x_1 + (1 - x_1) G_{31}} \right) \right) \\ &\quad + \ldots \frac{(1 - x_1) G_{13}}{x_1 G_{13} + (1 - x_1)} \left(\tau_{13} - \left(\frac{x_1 \tau_{13} G_{13}}{x_1 G_{13} + (1 - x_1)} \right) \right) \end{aligned} \tag{31}$$

$$\begin{aligned} &\ln(\gamma_3) \\ &= \frac{\tau_{13} G_{13} x_3 + \tau_{23} G_{23} x_2 + \tau_{33} G_{33} x_3}{G_{13} x_1 + G_{23} x_2 + G_{33} x_3} \\ &\quad + \ldots \frac{x_1 G_{31}}{x_1 + (1 - x_1) G_{31}} \left(\tau_{31} - \left(\frac{x_3 \tau 31 G_{31}}{x_1 + x_3 G_{31}} \right) \right) \\ &\quad + \ldots \frac{(1 - x_1)}{x_{1 G_{13}} + (1 - x_1)} \left(- \left(\frac{x_1 \tau_{13} G_{13}}{x_1 G_{13} + (1 - x_1)} \right) \right) \end{aligned} \tag{32}$$

In addition, we used the Antoine equation to calculate the pure component vapor pressures, P^0, for ethanol and water,

$$ln(P_1^0) = 16.5726 - \frac{3576.89}{T - 50.35} \tag{33}$$

$$ln(P_3^0) = 16.2887 - \frac{3814.43}{T - 45.98} \tag{34}$$

The pressure of the system, P, is constant at 101.325 kPa, therefore for any T, between the saturation temperature of ethanol and water, there is a real solution for the thermodynamic equilibrium variables ($\gamma_1, x_1, y_1, \gamma_3, P$).

e: VAPOR-LIQUID EQUILIBRIUM (METHANOL-ETHANOL-WATER)

The same water-ethanol equations are applicable. The extended Raoult's Law gives the equilibrium between the vapor and liquid phases:

$$P_2^0 \gamma_2 x_2 = P y_2 \tag{35}$$

and the methanol vapor pressure, P_2^0, by the Antoine equation,

$$\ln\left(P_2^0\right) = 16.5726 - \frac{3624.53}{T - 34.14} \tag{36}$$

The NTRL activity model (coefficients shown in Table 1) for methanol is given by

$$\begin{aligned} &Ln(\gamma_2) \\ &= \frac{\tau_{12} G_{12} x_1 + \tau_{32} G_{32} (1 - x_1)}{G_{12} x_1 + G_{32} (1 - x_1)} \\ &\quad + \ldots \frac{x_1 G_{21}}{x_1 + (1 - x_1) G_{31}} \left(\tau_{21} - \left(\frac{\tau_{31} G_{31} (1 - x_1)}{x_1 + (1 - x_1) G_{31}} \right) \right) \\ &\quad + \ldots \frac{(1 - x_1) G_{23}}{x_1 G_{13} + (1 - x_1)} \left(\tau_{23} - \left(\frac{\tau_{13} G_{13} x_1}{x_1 G_{13} + (1 - x_1)} \right) \right) \end{aligned} \tag{37}$$

5) RELATIONSHIPS FOR MEASURED VARIABLES

Because relevant state variables cannot be measured directly in the pilot plant, post-processing of some simulation variables is needed to compare the measured experimental data with the simulation predictions. The measurements were sensitive to temperature changes; therefore, for practical reasons, the distillate is assumed under standard conditions ($T_d = 298$ K, $P_d = 101.325$ kPa).

The distillate volumetric ethanol concentration, A_d, which is measured online (%v/v or GL°) with the density sensor, is given by

$$A_d = \left(1 + \frac{1 - y_{1,d}}{y_{1,d}} \frac{MW_3}{MW_1} \frac{\rho_1(T_d)}{\rho_3(T_d)} \right)^{-1} 100 \tag{38}$$

The molar flow rate, D, is given by the measured distillate volumetric flow rate, F_d, and the liquid density evaluated at the distillate conditions, $\rho(y_{1,d}, T_d)$,

$$D = \frac{F_d \rho(y_{1,d}, T_d)}{\left(MW_1 y_{1,d} + \left(1 - y_{1,d} \right) MW_3 \right)} \tag{39}$$

D. PREPARATION OF MODEL FOR CODING

1) ALGEBRAIC MANIPULATION

The model equations presented in Section II.C were manipulated to yield an almost explicit form so that conventional ODE solvers in MATLAB /Simulink could be used, thereby simplifying the numerical solving strategy. The following steps were performed to obtain an explicit ODE system.

a: EXPLICIT WATER-ETHANOL VLE

Following previous work [21], an efficient method was applied where the phase equilibrium equations were presolved, and later the unique real solution was fitted to several polynomials, avoiding solving the nonlinear equations each integration time step.

In our case, the set of nonlinear equations given by Dalton's Law, Raoult's Law, and NTRL activity coefficients (29-33) was pre-solved using the fsolve solver in MATLAB for a set of temperature values. This temperature set was given by a linearly spaced vector of 100 elements delimited by the ethanol and water saturation temperatures at 101.325 kPa (352-373 K).

Then, from the matrix of values obtained, the vectors of the variables of interest are conveniently extracted in pairs to fit

the next set of polynomials:

$$y_1 = \begin{cases} 0.5145T^2 - 365.04T + 63693 & T \leq 351.89 \\ -0.0003T^3 + 0.3199T^2 \ldots & \\ \quad -114.91T + 13760 & 351.89 < T < 362 \\ -0.0337T + 12.596 & 362 \leq T \end{cases} \tag{40}$$

$$y_1 = \frac{1.498 + 1220(x_1^*) - 735.1(x_1^*)^2 + 1220(x_1^*)^3}{113 + 1538(x_1^*) + 54.93(x_1^*)^2 + (x_1^*)^3} \tag{41}$$

$$x_1^* = \frac{1}{179.6 - 865(y_1) + 1586(y_1)^2 - 1299(y_1)^3 + 400(y_1)^4} \tag{42}$$

$$T = \frac{374.1 + 5855x_1^*}{1 + 16.65x_1^* + 0.01086\left(x_1^*\right)^2} \tag{43}$$

$$T = \frac{396.6 - 863.6y_1 + 1049\,(y_1)^2}{1 - 2.34y_1 + 2.9818\,(y_1)^2} \tag{44}$$

Our criterion was to choose the simplest polynomial that yielded an average relative error of <1%.

b: REARRANGEMENT OF THE REBOILER ODE'S

The relevant state variables in this section are: $[M_b, x_{1,b}, x_{2,b}]$, described in (1-3). Through algebraic manipulation applying the linearity property of the derivatives and the chain rule, it was possible to obtain three explicit ODE for each state variable:

$$\frac{dM_b}{dt} = f_1(\boldsymbol{x}, \boldsymbol{w}, \boldsymbol{u}, \boldsymbol{\theta}) \tag{45}$$

$$\frac{dx_{1,b}}{dt} = f_2(\boldsymbol{x}, \boldsymbol{w}, \boldsymbol{u}, \boldsymbol{\theta}) \tag{46}$$

$$\frac{dx_{2,b}}{dt} = f_3(\boldsymbol{x}, \boldsymbol{w}, \boldsymbol{u}, \boldsymbol{\theta}) \tag{47}$$

The boiler energy balance (4) is reduced to an explicit algebraic expression for the vapor flow rate, V_b, following the ''dynamic distillation derivative'' method described in [52].

c: TRANSFORMATION OF A PDE SYSTEM INTO AN ODE SYSTEM

The method of lines (MOL) was applied as spatial discretization to transform the PDEs into an ODE system [53], [54]. The first step is to apply the chain rule to the left-hand side equation of the packed column mass and energy balances (5-8). Hence, the mass matrix α, whose elements are nonlinear functions of the state variables, yields an explicit PDE system. Therefore, the convective term, $\frac{\partial f(\mathbf{Y})}{\partial z}$, is discretized with the upwind scheme following the direction of the liquid velocity; then, the difference is evaluated at each i and previous $i-1$ discrete element. The source term $\mathbf{R}$, and the mass matrix, are evaluated at each discrete element. The expression resulting from this transformation method is given by,

$$\boldsymbol{\alpha}\frac{d\mathbf{Y}}{dt} = \frac{\partial f(\mathbf{Y})}{\partial z} + \boldsymbol{R}\frac{d\mathbf{Y_i}}{dt} = \left(\frac{f(\mathbf{Y_i}) - f(\mathbf{Y}_{i-1})}{\Delta z} + \mathbf{S}_i\right)\boldsymbol{\alpha}_i^{-1} \tag{48}$$

The column height (28 cm) was discretized into $n = 7$ elements, giving slices of 4 cm each, matching the position of the temperature sensors. The boundary conditions in the packed column were of the Dirichlet type (Table 2).

TABLE 2. Boundary conditions for the packed column.

$z = 0$ (Reboiler)	$z = l$ (Partial Condenser)
$V = V_b$	$L = L_c$
$y_1 = y_{1,b}$	$x_1 = x_{1,c}$
$y_2 = y_{2,b}$	$x_2 = x_{2,c}$
$T = T_b$	$T = T_c$

This ODE system was rearranged following the same procedure applied to the reboiler equations, resulting in a set of $4n = 28$ explicit ODEs $\forall i = [1, 2, \ldots, n]$,

$$\frac{dM_i'}{dt} = f_{4i}(\boldsymbol{x}, \boldsymbol{w}, \boldsymbol{u}, \boldsymbol{\theta}) \tag{49}$$

$$\frac{dx_{1,i}}{dt} = f_{4i+1}(\boldsymbol{x}, \boldsymbol{w}, \boldsymbol{u}, \boldsymbol{\theta}) \tag{50}$$

$$\frac{dx_{2,i}}{dt} = f_{4i+2}(\boldsymbol{x}, \boldsymbol{w}, \boldsymbol{u}, \boldsymbol{\theta}) \tag{51}$$

$$\frac{dT,i}{dt} = f_{4i+3}(\boldsymbol{x}, \boldsymbol{w}, \boldsymbol{u}, \boldsymbol{\theta}) \tag{52}$$

d: REARRANGEMENT OF VAPOR PHASE EQUATIONS

The vapor-phase molar fractions of ethanol and methanol in the packed column were described using two ODEs (9-10). Discretization was also applied to these equations, resulting in $2n = 14$ additional algebraic equations. After some algebra, it is possible to obtain explicit algebraic equations to calculate the vapor flow rates, V_i, in the packed column, which depends on the previous element flow rate, V_{i-1}; thus, at the first element it is needed the reboiler vapor flow rate, V_b.

e: REARRANGEMENT OF THE PARTIAL CONDENSER ALGEBRAIC EQUATIONS

In this case, (11-15) were combined with the heat transfer relation (20), resulting in a reduced system of two implicit algebraic equations in the unknown variables $\left[x_{1,c}, T_{w.out}\right]$,

$$0 = h_1(\boldsymbol{x}, \boldsymbol{w}, \boldsymbol{u}, \boldsymbol{\theta}) = V_n H_n - L_c h_c - \ldots DH_D - h_w A_c \phi_{heat} \frac{T_{w,out} - T_{w,in}}{Ln\left(\frac{T_c - T_{w,in}}{T_c - T_{w,out}}\right)} \tag{53}$$

$$0 = h_2(\boldsymbol{x}, \boldsymbol{w}, \boldsymbol{u}, \boldsymbol{\theta}) = T_{w,out} - \ldots \left(T_c - \left(T_c - T_{w,in}\right)\exp\left(\frac{-h_w A_c \phi_{heat}}{F_w \rho_w c_{p,w}}\right)\right) \tag{54}$$

These are highly coupled to the state variables in this section; therefore, both equations must be solved simultaneously at each integration step.

2) NUMERICAL SOLUTION AND SIMULATION

The resulting differential-algebraic equation (DAE) system is highly nonlinear, comprising $3 + 4n = 31$ ODEs (55), two implicit algebraic equations (56), and 113 explicit algebraic equations, characterized by vectors $\boldsymbol{f}$ (57) and $\boldsymbol{h}$ (58), respectively; this problem structure is typical of distillation system with packed columns [55]. States are represented by (59), implicit variables by (60), and input variables by (61), which include the manipulated variables and measured disturbance $T_{w.in}$. The four model parameters in (62) were regressed from the experimental data. A consistent initial condition is obtained by solving (55) and (56) simultaneously at steady-state (zeros on the left-hand side).

$$\dot{\boldsymbol{x}} = \frac{d\boldsymbol{x}}{dt} = \boldsymbol{f}(\boldsymbol{x}, \boldsymbol{w}, \boldsymbol{u}, \boldsymbol{\theta}) \tag{55}$$

$$0 = \boldsymbol{h}(\boldsymbol{x}, \boldsymbol{w}, \boldsymbol{u}, \boldsymbol{\theta}) \tag{56}$$

$$\boldsymbol{f} = [f_1, \ldots, f_{4n}, f_{4n+1}, f_{4n+2} f_{4n+3}]^T \tag{57}$$

$$\boldsymbol{h} = [h_1, h_2]^T \tag{58}$$

$$\boldsymbol{x} = [M_b, x_{1b}, x_{2b}, M'_1, x_{1,1}, x_{2,1}, T_1, \ldots, M'_{4n}, x_{1,4n}, x_{2,4n}, T_{4n}]^T \tag{59}$$

$$\boldsymbol{w} = \left[x_{1,c}, T_{w.out}\right]^T \tag{60}$$

$$\boldsymbol{u} = [Q_b, F_w, T_{w.in}]^T \tag{61}$$

$$\boldsymbol{\theta} = \left[M'_{shell} Cp_{shell}, \phi_{mass}, \phi_{heat}, Q'_{loss}\right]^T \tag{62}$$

$$\boldsymbol{x}(t=0) = \boldsymbol{x_0}; \quad \boldsymbol{h}(t=0) = \boldsymbol{h_0} \tag{63}$$

$$\boldsymbol{v} = \boldsymbol{g}(\boldsymbol{x}, \boldsymbol{w}, \boldsymbol{u}, \boldsymbol{\theta}) \tag{64}$$

$$\boldsymbol{v} = [A_d, D]^T \tag{65}$$

$$\boldsymbol{g} = [g_1, g_2]^T \tag{66}$$

One option to solve this system is to embed an implicit equation solver (`fsolver` or `fzero`) nested with the ODE solver. However, this method is computationally expensive because it requires solving the implicit algebraic system at each integration step, and there is always the possibility of constraint drift. Rearranging the implicit algebraic equations to reduce the DAE index is a better option. In our model, we replaced the two implicit algebraic equations with two new ODEs to obtain a DAE system of index zero [56]. This procedure applies the implicit derivation theorem (the "index reduction" method), which requires extensive algebraic manipulation and yields complicated algebraic expressions since a large symbolic Jacobian matrix must be inverted. Moreover, determining suitable initial conditions for the new ODEs is challenging.

We found that the best option to solve our model was to use an algebraic loop constraint function block within MATLAB/Simulink. In this case, the implicit equations and the ODEs are solved simultaneously, although a semi-explicit DAE solver should be applied [45], [46]. The integrator chosen was `ODE15s` [57], which is appropriate for DAE (index 1) and stiff systems. To check the DAE index order in our model, we compute the algebraic matrix rank of the Jacobian of $\boldsymbol{h}$ with respect to $\boldsymbol{w}$, obtaining a full rank (all linearly independent rows) for any discretization size form $n = 1$ to 7, therefore our DAE index is 1. The implementation of the solution method in Simulink using the algebraic loop scheme is shown in Fig. 5.

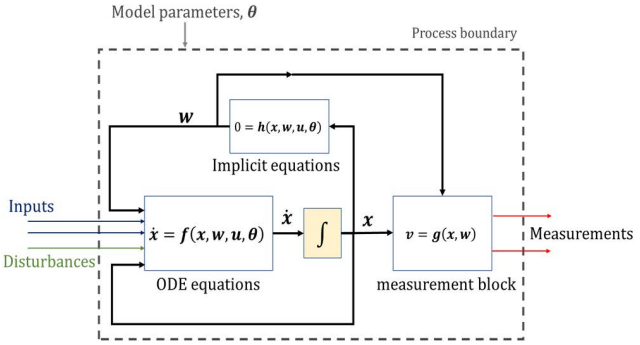

FIGURE 5. The batch distillation packed column model solution method in Simulink.

This method uses a feedback loop for the implicit variables considered inputs to the ODE system. In our case, this strategy was 60 times faster than solving implicit equations using an embedded nonlinear solver. Simulink has robust algorithms for handling loops, as they typically appear in feedback control and other applications that include signal recirculation.

We also analyzed other solving strategies for PDEAs; however, most of them focus on linear PDEs [41], [43], [44], which are not suitable for our model. An appealing alternative solution for nonlinear PDEAs is described in [42] for a chromatography column (one PDE, one ODE, and one implicit algebraic equation), taking 10 times less CPU time than the method of lines (the strategy we used in this study); however, our model is larger (three ODE, four PDE, and two implicit equations); moreover, nonlinearities are much more complex.

Additional features such as variable scaling and smoothing of discontinuities are necessary to achieve robust and efficient simulations. Scaling was necessary to improve the solver performance [47], given the significant differences in the order of magnitude of the model variables, that is, temperatures on the order of 10^2, ethanol molar fractions on the order of 10^{-1} and methanol molar fractions on the order of 10^{-4}. A linear scaling procedure was implemented, which set all state variables to remain approximately between the limit values $a = -1$ and $b = 1$. Therefore, the scaled variable, x_{scaled}, and the variable in engineering units, x, are related by

$$x_{scaled} = \left(\frac{b-a}{x_{rng}}\right)(x - x_{ss}) \tag{67}$$

$$x = \left(\frac{x_{rng}}{b-a}\right) x_{scaled} + x_{ss} \tag{68}$$

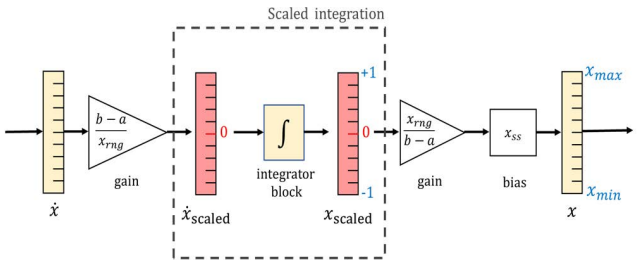

FIGURE 6. Scaling of variables for the integration.

When the derivative of a scaled variable is required, it can be easily obtained by derivation of (67) to obtain,

$$\dot{x}_{scaled} = \left(\frac{b-a}{x_{rng}}\right)\dot{x} \tag{69}$$

The parameters involved in the scaling process are the variable range, x_{rng}, and reference value x_{ss}, which depend on the approximate maximum and minimum variable values anticipated in the experiment.

$$x_{rng} = x_{max} - x_{min} \tag{70}$$

$$x_{ss} = 0.5\,(x_{max} + x_{min}) \tag{71}$$

This scaling methodology, as shown in Fig. 6, is widely used in data analytics because it improves the numerical conditioning of the problem and eases the setting integration error tolerances of the ODE solver.

Numerical tests found that it was crucial to smooth the model discontinuities to attain robust simulations and prevent the failure of the implicit solvers. The model discontinuities include the piecewise nature of the Nusselt number correlation (20) and the vapor/liquid equilibrium calculations in the vapor phase (40). These expressions generate numerical difficulties at the transition points, waste time in unnecessary iterations, and can cause complete failure of the integration. A simple method was implemented, smooth sigmoidal transitions, where two functions f_1 and f_2 are multiplied by a variable weight β, described in (72) and (73). Two parameters must be specified: the value when the transition occurs, $x_{transition}$, and a tuning parameter, $\Delta x_{transition}$, which defines the transition steepness. This procedure avoids solver failures.

$$f_{smooth}(x) = f_1(x)(1-\beta(x)) + f_2(x)\beta(x) \tag{72}$$

$$\beta(x) = \frac{1}{1+\exp\left(\frac{-(x-x_{transition})}{\Delta x_{transition}}\right)} \tag{73}$$

On average, the complete distillation model takes 1.8 s to run an open-loop simulation without disturbances in MATLAB/Simulink Online R2020a (Intel Xenon Platinum 8178M). Alternatively, an Intel i7-8700K desktop computer with MATLAB R2020a takes 1.07 seconds. For comparison, a preliminary version of our model was run with the implicit equations solved at each time step, without scaling and no smoothing transitions; it took 10 min to run the same open-loop simulation.

III. RESULTS AND DISCUSSION

The four free model parameters in (62) were regressed by minimum least-squares using a global optimization algorithm. We choose a global over a local solver given our model's strong nonlinearities and multiple free parameters, making it prone to falling into a local optimum. The experimental data were obtained using the pilot-scale batch distillation column described in Section II.A. Additionally, sensitivity and residues analyses were performed to assess the model's performance.

A. EXPERIMENTAL DISTILLATION DATA SET

The reboiler was initially loaded with 40 L of a water and ethanol mixture (13% v/v) and then heated at a constant rate ($Q_b = 1000$ W) until the end of distillation. A set of similar distillations was carried out, keeping the heat removed by the partial condenser constant at 140 W (#1 and #2), 200 W (#3 and #4), and 250 W (#5 and #6). The partial condenser heat was controlled with a steady-state feedforward strategy derived from an energy balance, which manipulated the cooling water flow rate, F_w, and measured its inlet and outlet temperatures. The datasets were split into calibration runs (#1, #2, #5, and #6) and validation runs (#3 and #4).

The sample time was 10 s, and the process variables were recorded in LabView using National Instruments input/output modules, following the setup details of our previous work [30]. In addition, the recorded data was smoothed with a first-order filter with a time constant of 5 s, which was enough to reduce the sensor noises without extensive impact on the dynamic response of F_w and $T_{w,in}$.

B. MODEL CALIBRATION

The differences between the simulations and measurements of the distillate ethanol concentration, A_d, and outlet water cooling temperature, $T_{w,out}$, were considered in the cost function for model calibration.

The primary estimated parameters, $\boldsymbol{\theta}$, are given in (62). The initial ethanol concentration, $x_{1b,ini}$, was also estimated because it is difficult to precisely determine the ethanol concentration when the mixture starts boiling and distilling. Therefore, the actual vector of regressors is,

$$\boldsymbol{\theta} = \left[M'_{shell}Cp_{shell}, \phi_{mass}, \phi_{heat}, Q'_{loss}, x_{1b,0}\right]^T \tag{74}$$

It was necessary to tune the ODE/DAE integration option parameters to avoid simulation failures, considering that thousands of parameter combinations were evaluated during model calibration. A reliable set of integration parameters for our simulations with scaled variables was as follows: integration solver `ode15s`, max step size 10 s, absolute tolerance 10^{-3}, relaxed relative tolerance 10^{-2}.

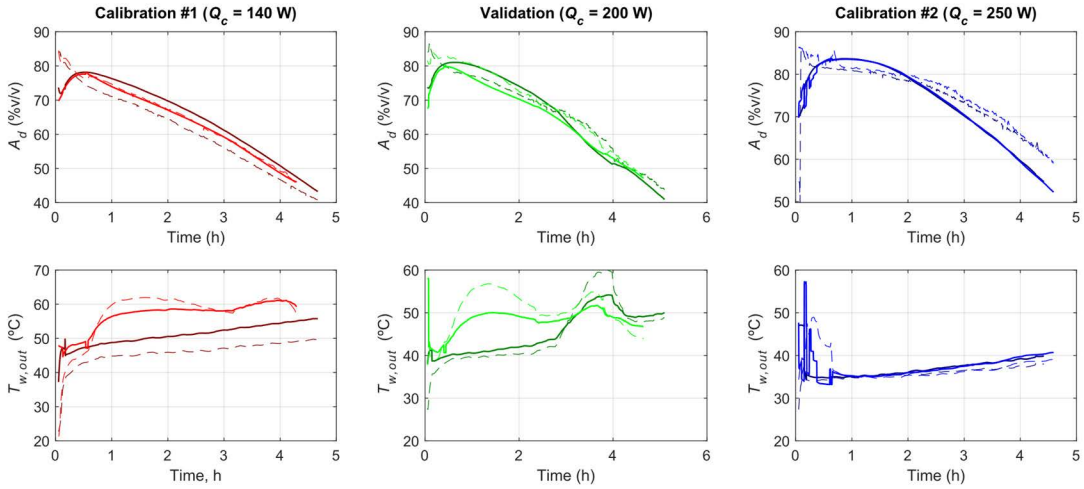

FIGURE 7. Experimental data set (segmented lines) of the calibration and validation, and comparison with model (continuous lines). Left graphs at $Q_c = 140$ W (calibration data) shows Run #1 (red) and Run #2 (dark red). Middle graphs at $Q_c = 200$ W (validation data) shows Run #3 (green) and Run #4 (dark green). Right graphs at $Q_c = 250$ W (calibration data) shows Run #5 (blue) and Run #6 (dark blue).

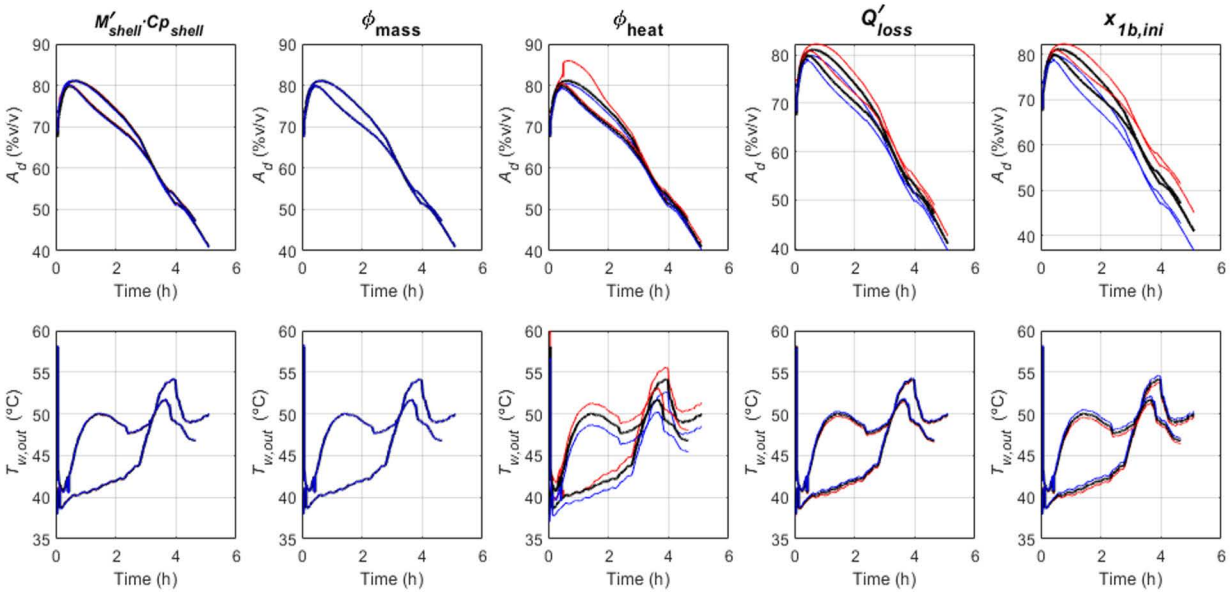

FIGURE 8. Sensitivity parameter analysis at validation model conditions ($Q_c = 200$ W; Run #3 and #4). The continuous lines are the simulations as follows: nominal parameter value (black),+10% (red) and -10% (blue).

The fitted parameter vector is given by the argument that minimizes,

$$\hat{\boldsymbol{\theta}} = arg\min_{\boldsymbol{\theta}} \omega \sum_k^m \sum_i^{n_k} \left(\frac{A_{d_{ik}}^{model} - A_{d_{ik}}^{exp}}{n_k \max\left(A_{d_k}^{exp}\right)} \right)^2 + \ldots (1-\omega) \sum_k^m \sum_i^{n_k} \left(\frac{T_{w,out_{ik}}^{model} - T_{w,out_{ik}}^{exp}}{n_k \max\left(T_{w,out_k}^{exp}\right)} \right)^2 \tag{75}$$

This nested minimization corresponds to each experimental run's weighted normalized mean square error (NMSE). Subindex i refers to the observations ($n_k = 1700$ samples) and k refers to the m experimental runs ($m = 4$; 2 for each duplicate for 140 and 250 W). The cost function errors were normalized by the maximum experimental value and number of data points in the corresponding experimental run. In addition, the weight ω was set by trial and error, beginning with weight values of 0.5; however, the results showed poor performance of both variables. Consequently, it was

finally fixed to 0.9 to prioritize a better fit on A_d (which has a significant impact on spirits quality) over $T_{w,out}$. Once the cost function is defined, and the experimental data is split, the optimization problem can be solved.

The scatter-search global optimization package *MEIGO* [58], [59] was used to solve (75). The solver converged in a reasonable time (1 h) after tuning several solver parameters such as the number of diversifications = 40, max number of evaluations = 500, and local solver algorithm = `fmincon`. We also compare the results and performance with other tools, such as the global search function `GlobalSarch` of the MATLAB Global Optimization Toolbox. Similar calibration results were obtained, although taking much longer to run (6 h) and to tune the solver parameters.

The model performance indices (NMSE) for each calibration and validation experiment are given in Table 3. The calibrated parameter values are listed in Table 4.

TABLE 3. Model performance indices: calibration and validation.

Run	Q_c	NMSE A_d $\cdot 10^{-3}$	NMSE $T_{w,out}$ $\cdot 10^{-3}$	Weighted NMSE $\cdot 10^{-3}$
#1	140 W	3.47	12.81	4.40
#2	140 W	0.82	4.60	1.20
#3	200 W	1.51	2.00	1.56
#4	200 W	1.86	5.82	2.26
#5	250 W	2.25	5.95	2.26
#6	250 W	2.81	5.90	3.11

The time series plots in Fig. 7 illustrate the model's capability more clearly than the performance indices. Calibration #1 shows a significant and rather constant bias for A_d in Run #2, while A_d fitting in Run #1 was almost perfect. A_d biases for Run #5 and Run #6 in Calibration #2 are larger and increase with time. In this case, a model parameter probably changes its value at high distillation rates. Interestingly, the average ethanol concentration predictions in the validation experiments were the best.

$T_{w,out}$ bias in Calibration #1 is almost constant in Run #1; in Run #2, a significant bias only appears between 1.8 and 2.8 h. In the validation case, a significant bias is noticed in Run #4 only between 3.1 and 4 h, while Run #3 presents a significant and variable bias between 0. 5 and 3.7 h and after 4.1 h. The outlet water temperature appears highly sensitive to unacquainted disturbances, which explains the observed dynamics variability and prediction biases. The temperature fitting for Calibration #2 was almost perfect, and both experimental runs were very much alike; hence, unmeasured disturbances seem neglectable in these experiments.

It is important to notice that simulations at the beginning of the distillations are unreliable, and this limitation is probably due to the difficulties of establishing reliable initial conditions for the simulations.

TABLE 4. Regressed parameter values.

Parameter	Value	Units
$M'_{shell}Cp_{shell}$	2.7914e+05	J/(ºC·m)
ϕ_{mass}	0.853	-
ϕ_{heat}	0.306	-
$Q_{loss}{}'$	27.17	W/m
$x_{1b,ini}$	0.0431	-

C. SENSITIVITY ANALYSIS

Rigorous analysis needs a fully explicit ODE system to obtain the sensitivity matrix [60], [61], [62]. We applied a more straightforward approach for the sensitivity analysis of the DAE batch distillation model. The impact of each estimated parameter on the measured variables was assessed by changing their nominal values by $\pm 10\%$ in two simulations based on the condition of distillations #Run 3 and #Run 4.

The model output variables observed for this sensitivity analysis were the ethanol concentration and the outlet temperature, as shown in Fig. 8. The least sensitive parameters for both output variables are $M'_{shell}Cp_{shell}$ and ϕ_{mass}; it is observed that at the operating point and for that level of variation, these parameters do not play any relevant role. The most sensitive parameter for ethanol concentration is Q'_{loss}, suggesting that heat losses cause additional condensation, thus impacting the compositions in the column. The most sensitive parameter for the outlet coolant temperature is ϕ_{heat}, because that parameter has a direct impact on the heat transfer efficiency. Finally, the sensitivity of the initial condition of ethanol in the boiler, $x_{1b,ini}$, was also analyzed. As expected, this initial condition greatly impacts the ethanol concentration because it defines the initial ethanol availability.

D. ANALYSIS OF RESIDUALS

This analysis can provide insights on modifying or extending the model to improve its performance. The residuals of an ideal model should be randomly distributed, show no structure, and be time-independent [63], [64], [65], [66].

A validation data set (different from the calibration set) was used to test the model residuals. We used the 200 W experimental data sets (runs # 3 and #4) to analyze the residuals.

The structure of the residuals was verified by plotting their evolution (Fig. 9). The residuals distribution was analyzed using the normality probability plots (NPP), shown in Fig. 10.

Ideally, no time structure should be observed in the evolution of the residual with zero mean and homogenous dispersion [67]. The ethanol concentration residuals in both the experiments and the temperature residual in run #4 showed a similar pattern (Fig. 9): an exponential decline at the beginning, followed by a low-frequency oscillation. The temperature residuals in run #3 were much less variable. The large deviations at the beginning suggest that other phenomena should be included in the model to reproduce the distillation process's start-up better.We believe that the low frequency oscillations observed within 0.5 – 5 h were caused by an unmeasured disturbance, such as the ambient temperature.

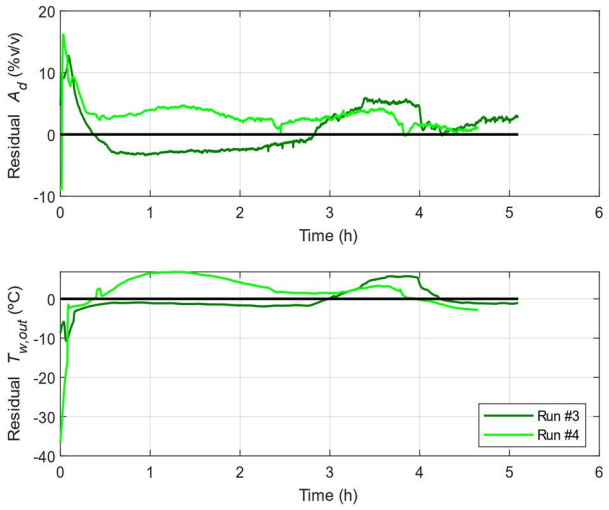

FIGURE 9. Evolution of the residuals for distillations with $Q_c = 200$ W heat-removal. Continuos lines for Run #3 (green) and Run #4 (dark green).

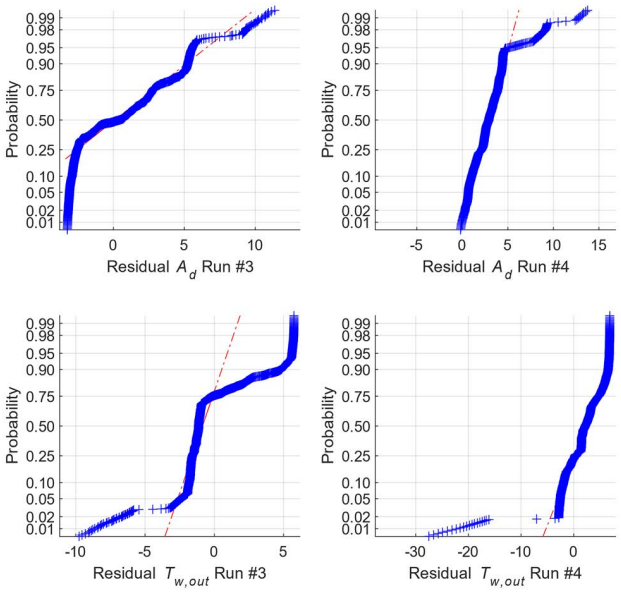

FIGURE 10. Normality probability plots for distillations with 200 W heat-removal. Left graphs for Run #3 and right graphs for Run #4. The points are for the residuals (blue), and the best normality trend is shown with a segmented line (red).

A more detailed heat-loss model can include the impact of this temperature on the simulation outputs.

The Anderson-Darling (A-D) test, available in MATLAB (`adtest`), was applied to verify the probability distribution of the residuals. This routine calculates the residual accumulated probability of the NPPs and the corresponding p-values. According to this test, the two experiments' residuals do not follow a normal distribution ($p < 0.05$; 95% confidence). Figure 10, where the segmented red lines represent the normal distribution, confirms that the residuals deviated significantly from normality and that there were many outliers due to unmodelled dynamics. Nevertheless, the ethanol concentration residuals are closer to the normal distribution than the temperature residuals. This analysis supports that the heat transfer model may be improved.

E. MODIFIED HEAT LOSS MODEL

To verify if a variable heat-loss model could better represent the batch column dynamics, we ran an additional experimental distillation operating the partial condenser in an open loop, applying a sequence of step changes in F_w. The experiment was performed under the same operating conditions as previously set: $Q_b = 1000$ W, loaded volume = 40 L, and ethanol concentration of the loaded mixture = 13% v/v.

The new model includes two additional fitting parameters: the overall heat-loss parameter associated with the packed column, UA'_{loss}, and the overall heat loss parameter associated with the partial condenser, UAc_{loss}. The corresponding temperature differences were the ambient temperature, T_{amb}, (considered constant at 25 °C) minus the packed column temperature, T_i, or the partial condenser temperature, T_c. Hence, the new heat-loss model includes the following equations.

$$Q'_{loss_i} = UA'_{loss}(T_{amb} - T_i) \tag{76}$$

$$Q_{loss_c} = UAc_{loss}(T_{amb} - T_c) \tag{77}$$

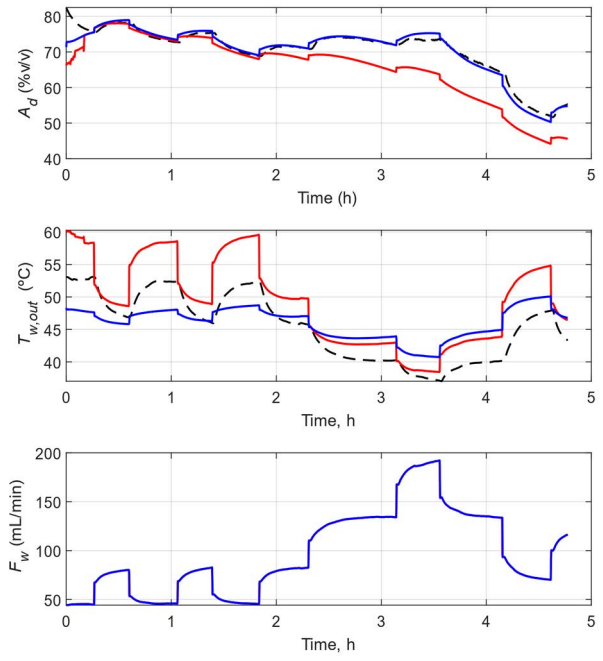

FIGURE 11. Comparing original (red) and new model (blue) in a variable cooling water flow rate distillation. The experimental data (black) is shown as a segmented line.

The new regression results are shown in Fig. 11; the ethanol concentration predictions were much better than those of the original model. The considerable bias after approximately 2 h shown in the simulations with the previous model was absent in the new model simulations. The partial condenser outlet temperature predictions improved with the new model,

TABLE 5. Performance and regressed parameters.

Parameter	Previous Model	Modified Model	Units
$M'_{shell}Cp_{shell}$	2.7914e+05	2.6949e+05	J/(ºC·m)
ϕ_{mass}	0.853	0.580	-
ϕ_{heat}	0.306	0.856	-
Q'_{loss}	27.17	-	W/m
UA'_{loss}	-	0.191	W/(ºC·m)
UAc_{loss}	-	2.772	W/(ºC)
$x_{1b,ini}$	0.0431	0.0397	-
NMSE Ad	0.0240	0.0046	-
NMSE Tout	0.0067	0.0042	-

although a significant bias remained. Hence, there are still disturbances and dynamic phenomena that have not yet been identified. The new set of free parameters was compared with the previous model fitting in Table 5. It should be considered that in the new simulation with the original model, we used the same model parameters fitted in the model calibration section.

As expected, the values of the new fitting parameters differed from the previous ones because the calibration data and model structures differed. The effective heat and mass transfer area were the most affected factors. As shown in Table 5, the performance indices associated with the new model reveal a significant improvement compared to those of the previous model. To explain this improvement, we analyzed the heat loss simulations, noting that the internal column temperature varied between 80 and 93 °C (data not shown). These column temperatures minus the ambient temperature of 25°C resulted in column heat losses between 10.5 and 12.8 W/m, which is less than half the value obtained in the previous model (27.17 W/m). Finally, we analyzed the heat loss in the partial condenser that occurred in the new model. It was verified that the heat loss in the partial condenser was between 150 and 190 W. Consequently, the coolant outlet temperature decreased, approaching the temperature measured in the experiments (middle graph in Fig. 11). Overall, this implies that a considerable amount of the total removed heat is not directly manipulable by coolant flow rate.

IV. CONCLUSION

A realistic model of a pilot-scale batch distillation column for fruit distillates, which has a challenging DAE system of index 1, was developed and solved efficiently. Despite the low index order, the solution was not trivial because of the strong nonlinearities and large size of the resulting model. Compared with previous simulations with similar models, the simulation times were reduced by two orders of magnitude. This reduction significantly simplified the model calibrations and performance analysis, yielding accurate predictions for distillate ethanol concentrations.

The heat transfer fitting parameters had the greatest influence on the model outputs. It was verified that the variable heat loss model significantly improved the predictions of distillate ethanol concentrations and outlet water temperatures.

TABLE 6. Variable list.

Variable	Definition	Units
L	Molar liquid Flow	mol/s
M	Mole of mixture	mol
V	Molar vapor flow	mol/s
D	Molar distillate flow	mol/s
N	Molar transfer flow	mol/s
x	Molar liquid fraction	-
y	Molar vapor fraction	-
h	Molar liquid enthalpy	J/mol
H	Molar Vapor enthalpy	J/mol
Q	Heat	J/s
T	Temperature	K
A	Volumetric ethanol concentration	%vol/vol
λ	Thermal conductivity	W/m·K
σ	Superficial tension	N/m
D_{ab}	Liquid diffusion coefficient	m^2/s
η	Kinematic viscosity	m^2/s
μ	Viscosity	Pa·s
ρ	Density	kg/m^3
V_{ap}	Apparent molar volume	m^3/mol
cp	Heat capacity	J/kg·K
Pr	Prandtl Number	-
Re	Reynolds Number	-
Gz	Graetz Number	-
Nu	Nusselt Number	-
h_L	Hydraulic load packed bed	-
u_L	Velocity liquid packed bed	m/s
S	Transversal section	m^2
P	Pressure	Pa
ϕ_{heat}	Efficiency factor heat transfer	-
ϕ_{mass}	Efficiency factor heat transfer	-
l	Length packed column	m
l_{eq}	Equivalent length	m
d_i	Partial condenser coil internal diameter	m
g	Gravity acceleration	m/s^2
a_{ef}	Effective interfacial packing area	m^2
γ	Activity coefficient	-
G, τ	NTRL coefficients	-
MW	Molecular weight	g/mol
n	Number of discretization stages	-
t	Time	s
z	Height	m
Δz	Discrete height element	
$\boldsymbol{\alpha}$	Mass matrix for example MOL	
$\boldsymbol{Y}$	State variable vector for example MOL	
$f(\boldsymbol{Y})$	Nonlinear function of convection for example MOL	
$\boldsymbol{R}$	Source term vector for example MOL	
$\boldsymbol{x}$	State variables vector	-
$\boldsymbol{w}$	Implicit variables vector	-
$\boldsymbol{u}$	Input variables vector	-
$\boldsymbol{\theta}$	Parameter vector	-

Even though the outlet water temperature simulations were somehow inaccurate, accurate predictions of ethanol concentrations are critical for process control and optimization because the recovery of valuable aromas in fruit distillations depends on the distillate ethanol content.

To improve the predictability of distillations, future development of this model should focus on developing a reliable procedure to define initial conditions, especially initial ethanol concentration in the boiler. Additionally, unmeasured disturbances and unmodelled dynamics affecting the partial condenser must be identified.

The model presented here helps design robust control systems and optimal operating strategies to enhance the recovery of valuable aromas, minimize toxic and undesirable volatile components in the distillate, and reduce the process's cooling water and energy consumption.

NOMENCLATURE

More details such as physical properties and the model code are available in the online repository: https://github.com/simondiaz5/batch-packed-column-fruit

TABLE 7. Subindex list.

Subindex	Definition
b	Reboiler section
c	Partial condenser section
d	Distillate stream
L	Liquid (bulk)
$loss$	Energy loss
$shell$	Cylindrical metal column shell
$fill$	Packing fill
i	Discrete element
w	Coolant water
in	Inlet
out	Outlet
0	Initial
n	The last discretized stage
lm	Logarithmic mean
vol	Volumetric

TABLE 8. Superindex list.

Superindex	Definition
$'$	Per longitudinal unit
$*$	Thermodynamic equilibrium
$\cdot$	Time derivative
0	Atmospheric pressure

ACKNOWLEDGMENT

The authors thank the Industrial Information Control Center at the University of Auckland for their technical support and advice. Finally, the written English edition by Lisa Gingles is highly appreciated.

REFERENCES

[1] J. Sacher, L. García-Llobodanin, F. López, H. Segura, and J. R. Pérez-Correa, "The spirit world: Can chemical engineering help spirits distillers close the loop between historic roots and modern modelling methods?" *Chem. Eng.*, no. 910, pp. 32–35, Apr. 2017. [Online]. Available: https://www.thechemicalengineer.com/magazine/issues/issue-910/

[2] E. Agosin, A. Belancic, A. Ibacache, R. Baumes, and E. Bordeu, "Aromatic potential of certain Muscat grape varieties important for Pisco production in Chile," *Amer. Soc. Enol. Viticulture*, vol. 51, no. 4, pp. 404–408, 2000.

[3] E. Bordeu, G. Formas, and E. Agosin, "Proposal for a standardized set of sensory terms for Pisco, a young muscat wine distillate," *Amer. Soc. Enol. Viticulture*, vol. 55, no. 1, pp. 104–107, 2004.

[4] D. W. Lachenmeier, F. Kanteres, and J. Rehm, "Carcinogenicity of acetaldehyde in alcoholic beverages: Risk assessment outside ethanol metabolism," *Addiction*, vol. 104, no. 4, pp. 533–550, Apr. 2009, doi: 10.1111/j.1360-0443.2009.02516.x.

[5] J. H. Thorngate, "Yeast strain and wine flavor: Nature or nurture?" in *Chemistry of Wine Flavor*, vol. 714, A. L. Waterhouse and S. E. Ebeler, Eds. Washington, DC, USA: ACS Symposium Series, 1998, pp. 66–80.

[6] A. Voilley and S. Lubbers, "Flavor-matrix interactions in wine," in *Chemistry of Wine Flavor*, vol. 714, A. L. Waterhouse and S. E. Ebeler, Eds. Washington, DC, USA: ACS Symposium Series, 1998, pp. 217–229.

[7] D. Heller and D. Einfalt, "Reproducibility of fruit spirit distillation processes," *Beverages*, vol. 8, no. 2, p. 20, Mar. 2022, doi: 10.3390/beverages8020020.

[8] G. Ferrari, O. Lablanquie, R. Cantagrel, J. Ledauphin, T. Payot, N. Fournier, and E. Guichard, "Determination of key odorant compounds in freshly distilled cognac using GC-O, GC-MS, and sensory evaluation," *J. Agricult. Food Chem.*, vol. 52, no. 18, pp. 5670–5676, Sep. 2004, doi: 10.1021/jf049512d.

[9] C. D. Porto, "Grappa and grape-spirit production," *Crit. Rev. Biotechnol.*, vol. 18, no. 1, pp. 13–24, Jan. 1998, doi: 10.1080/0738-859891224202.

[10] R. R. Madrera, A. P. Lobo, and J. J. M. Alonso, "Effect of cider maturation on the chemical and sensory characteristics of fresh cider spirits," *Food Res. Int.*, vol. 43, no. 1, pp. 70–78, Jan. 2010, doi: 10.1016/j.foodres.2009.08.014.

[11] J. Cacho, L. Moncayo, J. C. Palma, V. Ferreira, and L. Culleré, "Comparison of the aromatic profile of three aromatic varieties of Peruvian pisco (Albilla, Muscat and Torontel) by chemical analysis and gas chromatography-olfactometry: A comparison between aromatic varieties of Peruvian piscos," *Flavour Fragrance J.*, vol. 28, no. 5, pp. 340–352, Sep. 2013, doi: 10.1002/ffj.3171.

[12] M. P. Y. Lillo, E. Agosin, A. Belancic, and E. Latrille, "Chemical markers for tracking the sensory contribution of production stages in muscat wine distillates," *J. Food Sci.*, vol. 70, no. 7, pp. s432–s441, Sep. 2005.

[13] Y. Arrieta-Garay, P. Blanco, C. López-Vázquez, J. J. Rodríguez-Bencomo, J. R. Pérez-Correa, F. López, and I. Orriols, "Effects of distillation system and yeast strain on the aroma profile of Albariño (Vitis vinifera L.) grape pomace spirits," *J. Agricult. Food Chem.*, vol. 62, no. 43, pp. 10552–10560, Oct. 2014, doi: 10.1021/jf502919n.

[14] P. Matias-Guiu, J. J. Rodríguez-Bencomo, J. R. Pérez-Correa, and F. López, "Aroma profile design of wine spirits: Multi-objective optimization using response surface methodology," *Food Chem.*, vol. 245, pp. 1087–1097, Apr. 2018, doi: 10.1016/j.foodchem.2017.11.062.

[15] P.-R. Rogelio, G.-A. Victor, P.-O. Carlos, C. Norberto, E. Mirna, and G.-H. E. Héctor, "The role of distillation on the quality of tequila," *Int. J. Food Sci. Technol.*, vol. 40, no. 7, pp. 701–708, Aug. 2005, doi: 10.1111/j.1365-2621.2005.00983.x.

[16] L. García-Llobodanin, I. Achaerandio, M. Ferrando, C. Güell, and F. López, "Pear distillates from pear juice concentrate: Effect of lees in the aromatic composition," *J. Agricult. Food Chem.*, vol. 55, no. 9, pp. 3462–3468, May 2007, doi: 10.1021/jf0633589.

[17] L. F. Hernández-Gómez, J. Úbeda-Iranzo, E. García-Romero, and A. Briones-Pérez, "Comparative production of different melon distillates: Chemical and sensory analyses," *Food Chem.*, vol. 90, nos. 1–2, pp. 115–125, Mar. 2005, doi: 10.1016/j.foodchem.2004.03.033.

[18] A. Douady, C. Puentes, P. Awad, and M. Esteban-Decloux, "Batch distillation of spirits: Experimental study and simulation of the behaviour of volatile aroma compounds," *J. Inst. Brewing*, vol. 125, no. 2, pp. 268–283, 2019, doi: 10.1002/jib.560.

[19] M. M. Lopes and T. W. Song, "Batch distillation: Better at constant or variable reflux?" *Chem. Eng. Process., Process Intensification*, vol. 49, no. 12, pp. 1298–1304, Dec. 2010, doi: 10.1016/j.cep.2010.09.019.

[20] P. Matias-Guiu, J. J. Rodríguez-Bencomo, I. Orriols, J. R. Pérez-Correa, and F. López, "Floral aroma improvement of muscat spirits by packed column distillation with variable internal reflux," *Food Chem.*, vol. 213, pp. 40–48, Dec. 2016, doi: 10.1016/j.foodchem.2016.06.054.

[21] J. Carvallo, M. Labbe, J. R. Pérez-Correa, C. Zaror, and J. Wisniak, "Modelling methanol recovery in wine distillation stills with packing columns," *Food Control*, vol. 22, no. 8, pp. 1322–1332, Aug. 2011, doi: 10.1016/j.foodcont.2011.02.007.

[22] M. J. Claus and K. A. Berglund, "Fruit brandy production by batch column distillation with reflux," *J. Food Process Eng.*, vol. 28, no. 1, pp. 53–67, Feb. 2005, doi: 10.1111/j.1745-4530.2005.00377.x.

[23] J. J. Rodríguez-Bencomo, J. R. Pérez-Correa, I. Orriols, and F. López, "Spirit distillation strategies for aroma improvement using variable internal column reflux," *Food Bioprocess Technol.*, vol. 9, no. 11, pp. 1885–1892, Nov. 2016, doi: 10.1007/s11947-016-1776-0.

[24] N. Spaho, "Distillation techniques in the fruit spirits production," in *Distillation—Innovative Applications and Modeling*. London, U.K.: IntechOpen, 2017. [Online]. Available: https://www.intechopen.com/chapters/54078, doi: 10.5772/66774.

[25] L. García-Llobodanin, J. Roca, J. R. López, J. R. Pérez-Correa, and F. López, "The lack of reproducibility of different distillation techniques and its impact on pear spirit composition," *Int. J. Food Sci. Technol.*, vol. 46, no. 9, pp. 1956–1963, Sep. 2011, doi: 10.1111/j.1365-2621.2011.02707.x.

[26] W. Marquardt and M. Mönnigmann, "Constructive nonlinear dynamics in process systems engineering," *Comput. Chem. Eng.*, vol. 29, no. 6, pp. 1265–1275, May 2005, doi: 10.1016/j.compchemeng.2005.02.009.

[27] A. E. Rodrigues and M. Minceva, "Modelling and simulation in chemical engineering: Tools for process innovation," *Comput. Chem. Eng.*, vol. 29, no. 6, pp. 1167–1183, 2005, doi: 10.1016/j.compchemeng.2005.02.029.

[28] E. S. Lopez-Saucedo, I. E. Grossmann, J. G. Segovia-Hernandez, and S. Hernández, "Rigorous modeling, simulation and optimization of a conventional and nonconventional batch reactive distillation column: A comparative study of dynamic optimization approaches," *Chem. Eng. Res. Design*, vol. 111, pp. 83–99, Jul. 2016, doi: 10.1016/j.cherd.2016.04.005.

[29] F. Buzzi-ferraris and G. Manenti, *Differential and Diferencial-Algebraic System for the Chemical Engineer*. Weinheim, Germany: Wiley, 2013.

[30] S. D. Quezada, J. R. P. Correa, and M. A. F. Fernandez, "Automatic system distillation for wine fruit," *IEEE Latin Amer. Trans.*, vol. 13, no. 6, pp. 1882–1887, Jun. 2015, doi: 10.1109/TLA.2015.7164212.

[31] Y. Gu and W. Yuan, "Closed form solutions of nonlinear space-time fractional Drinfel'd-Sokolov-Wilson equation via reliable methods," *Math. Methods Appl. Sci.*, pp. 1–17, Jun. 2021, doi: 10.1002/mma.7868.

[32] Y. Gu, C. Wu, X. Yao, and W. Yuan, "Characterizations of all real solutions for the KdV equation and WR," *Appl. Math. Lett.*, vol. 107, Sep. 2020, Art. no. 106446, doi: 10.1016/j.aml.2020.106446.

[33] F. De Lucca, R. Munizaga-Miranda, D. Jopia-Castillo, C. A. Gelmi, and J. R. Pérez-Correa, "Operation strategies to minimize methanol recovery in batch distillation of hydroalcoholic mixtures," *Int. J. Food Eng.*, vol. 9, no. 3, pp. 259–265, Sep. 2013, doi: 10.1515/ijfe-2013-0031.

[34] D. Osorio, R. Pérez-Correa, A. Belancic, and E. Agosin, "Rigorous dynamic modeling and simulation of wine distillations," *Food Control*, vol. 15, no. 7, pp. 515–521, Oct. 2004, doi: 10.1016/j.foodcont.2003.08.003.

[35] D. Osorio, J. R. Pérez-Correa, L. T. Biegler, and E. Agosin, "Wine distillates: Practical operating recipe formulation for stills," *J. Agricult. Food Chem.*, vol. 53, no. 16, pp. 6326–6331, Aug. 2005, doi: 10.1021/jf047788f.

[36] R. Luna, P. Matias-Guiu, F. López, and J. R. Pérez-Correa, "Quality aroma improvement of muscat wine spirits: A new approach using first-principles model-based design and multi-objective dynamic optimisation through multi-variable analysis techniques," *Food Bioproducts Process.*, vol. 115, pp. 208–222, May 2019, doi: 10.1016/j.fbp.2019.04.004.

[37] R. Luna, F. López, and J. R. Pérez-Correa, "Minimizing methanol content in experimental charentais alembic distillations," *J. Ind. Eng. Chem.*, vol. 57, pp. 160–170, Jan. 2018, doi: 10.1016/j.jiec.2017.08.018.

[38] J. Sacher, L. García-Llobodanin, F. López, H. Segura, and J. R. Pérez-Correa, "Dynamic modeling and simulation of an alembic pear wine distillation," *Food Bioproducts Process.*, vol. 91, no. 4, pp. 447–456, Oct. 2013, doi: 10.1016/j.fbp.2013.04.001.

[39] F. Scanavini, R. Ceriani, and A. J. A. Meirelles, "Cachaça distillation investigated on the basis of model systems," *Brazilian J. Chem. Eng.*, vol. 29, no. 2, pp. 429–440, 2012, doi: 10.1590/S0104-66322012000200022.

[40] H. F. A. Scanavini and A. Meirelles, "Cachaça production in a lab-scale alembic: Modeling and computational simulation," *J. Food Process. Eng.*, vol. 33, no. 1, pp. 226–252, Feb. 2010, doi: 10.1111/j.1745-4530.2008.00352.x.

[41] W. Lucht, K. Strehmel, and C. Eichler-Liebenow, "Indexes and special discretization methods for linear partial differential algebraic equations," *BIT Numer. Math.*, vol. 39, no. 3, pp. 484–512, 1999, doi: 10.1023/A:1022370703243.

[42] Y. Il Lim, S. C. Chang, and S. B. Jørgensen, "A novel partial differential algebraic equation (PDAE) solver: Iterative space-time conservation element/solution element (CE/SE) method," *Comput. Chem. Eng.*, vol. 28, no. 8, pp. 1309–1324, 2004, doi: 10.1016/j.compchemeng.2003.09.016.

[43] W. Bao and Y. Song, "Multiquadric quasi-interpolation methods for solving partial differential algebraic equations," *Numer. Methods Partial Differ. Equ.*, vol. 30, no. 1, pp. 95–119, Jan. 2014, doi: 10.1002/num.21797.

[44] H. Chen, "A splitting preconditioner for implicit runge–kutta discretizations of a partial differential-algebraic equation," *Numer. Algorithms*, vol. 73, no. 4, pp. 1037–1054, Dec. 2016, doi: 10.1007/s11075-016-0128-5.

[45] L. F. Shampine, M. W. Reichelt, and J. A. Kierzenka, "Solving index 1 DAEs in MATLAB and Simulink," *Math. Comput. Sci.*, vol. 41, no. 3, pp. 538–552, 1999, doi: 10.1137/S003614459933425X.

[46] J. A. Kierzenka, "Manuscript of 'solving index-1 DAEs in MATLAB and 1062 simulink,'" Mathworks.com. Accessed: Aug. 1, 2022. [Online]. Available: https://la.mathworks.com/matlabcentral/fileexchange/7481-manuscript-of-solving-index-1-daes-in-MATLAB-and-simulink

[47] J. T. Betts, *Practical Methods for Optimal Control and Estimation Using Nonlinear Programming*. Philadelphia, PA, USA: Society for Industrial and Applied Mathematics, 2009.

[48] R. Luna, F. López, and J. R. Pérez-Correa, "Design of optimal wine distillation recipes using multi-criteria decision-making techniques," *Comput. Chem. Eng.*, vol. 145, Feb. 2021, Art. no. 107194, doi: 10.1016/j.compchemeng.2020.107194.

[49] R. Taylor and R. Krishna, *Multicomponent Mass Transfer*. New York, NY, USA: Wiley, 1993.

[50] E. N. Sieder and G. E. Tate, "Heat transfer and pressure drop of liquids in tubes," *Ind. Eng. Chem.*, vol. 28, no. 12, pp. 1429–1435, 1936, doi: 10.1021/ie50324a027.

[51] R. Billet and M. Schultes, "Predicting mass transfer in packed columns," *Chem. Eng. Technol.*, vol. 16, no. 1, pp. 1–9, Feb. 1993, doi: 10.1002/ceat.270160102.

[52] J. R. Bosley and T. F. Edgar, "An efficient dynamic model for batch distillation," *J. Process Control*, vol. 4, no. 4, pp. 195–204, 1994, doi: 10.1016/0959-1524(94)80041-3.

[53] Y.-T. Chen and J. Li, *Computational Partial Differential Equations Using MATLAB*. Boca Raton, FL, USA: CRC Press, 2008.

[54] W. E. Schiesser and G. W. Griffiths, *A Compendium of Partial Differential Equation Models: Method of Lines Analysis With Matlab*. Cambridge, U.K.: Cambridge Univ. Press, 2009.

[55] I. M. Mujtaba, *Batch Distillation: Design and Operation*, vol. 3. London, U.K.: Imperial College Press, 2004.

[56] C. C. Pantelides, D. Gritsis, K. R. Morison, and R. W. H. Sargent, "The mathematical modelling of transient systems using differential-algebraic equations," *Comput. Chem. Eng.*, vol. 12, no. 5, pp. 449–454, 1988, doi: 10.1016/0098-1354(88)85062-2.

[57] L. F. Shampine and M. W. Reichelt, "The MATLAB ODE suite," *SIAM J. Sci. Comput.*, vol. 18, no. 1, pp. 1–22, 1997, doi: 10.1137/S1064827594276424.

[58] M. Rodriguez-Fernandez, J. A. Egea, and J. R. Banga, "Novel metaheuristic for parameter estimation in nonlinear dynamic biological systems," *BMC Bioinf.*, vol. 7, no. 1, p. 483, Dec. 2006, doi: 10.1186/1471-2105-7-483.

[59] J. A. Egea, D. Henriques, T. Cokelaer, A. F. Villaverde, A. MacNamara, D.-P. Danciu, J. R. Banga, and J. Saez-Rodriguez, "MEIGO: An open-source software suite based on metaheuristics for global optimization in systems biology and bioinformatics," *BMC Bioinf.*, vol. 15, no. 1, pp. 1–9, Dec. 2014, doi: 10.1186/1471-2105-15-136.

[60] W. H. Wu, F. S. Wang, and M. S. Chang, "Dynamic sensitivity analysis of biological systems," *BMC Bioinf.*, vol. 9, no. S12, pp. 1–17, Dec. 2008, doi: 10.1186/1471-2105-9-S12-S17.

[61] C. A. Gelmi, J. Sacher, P. Saa, M. Cárcamo, J. López, and R. Pérez-Correa, "Improved calibration of a solid substrate fermentation model," *Electron. J. Biotechnol.*, vol. 14, no. 5, Sep. 2011, doi: 10.2225/vol14-issue5-fulltext-7.

[62] A. Perosa, M. Selva, V. Lucchini, M. Fabris, and M. Noé, "Kinetic parameter estimation of solvent-free reactions monitored by ^{13}C NMR spectroscopy, a case study: Mono- and Di-(hydroxy)ethylation of aniline with ethylene carbonate," *Int. J. Chem. Kinet.*, vol. 43, no. 3, pp. 154–160, 2011, doi: 10.1002/kin.20532.

[63] V. Mann, D. Maurya, A. K. Tangirala, and S. Narasimhan, "Optimal filtering and residual analysis in errors-in-variables model identification," *Ind. Eng. Chem. Res.*, vol. 59, no. 5, pp. 1953–1965, Feb. 2020, doi: 10.1021/acs.iecr.9b04561.

[64] J. P. Hessling, Ed., *Uncertainty Quantification and Model Calibration*. London, U.K.: IntechOpen, 2017. [Online]. Available: https://www.intechopen.com/books/5832, doi: 10.5772/65579.

[65] H. Stitt, M. Marigo, S. Wilkinson, and T. Dixon, "How good is your model?" *Johnson Matthey Technol. Rev.*, vol. 59, no. 2, pp. 74–89, Apr. 2015, doi: 10.1595/205651315X686804.

[66] J. Wisniak and A. Polishuk, "Analysis of residuals—A useful tool for phase equilibrium data analysis," *Fluid Phase Equilib.*, vol. 164, no. 1, pp. 61–82, 1999, doi: 10.1016/S0378-3812(99)00246-0.
[67] A. Rasmuson, B. Andersson, L. Olsson, and R. Andersson, *Mathematical Modeling in Chemical Engineering*. New York, NY, USA: Cambridge Univ. Press, 2014.

SIMÓN DÍAZ-QUEZADA was born in Santiago, Chile, in 1990. He received the degree in chemical engineering from the Universidad Tecnologica Metropolitana, Santiago, in 2014. He is currently pursuing the Ph.D. degree in science engineering-chemical and bioprocess engineering with the Pontificia Universidad Católica de Chile. His main research interests include modeling, simulation, optimization, and automatic control of chemical processes and bioprocesses.

DAVID I. WILSON received the B.E. degree in chemical and mathematics engineering from The University of Auckland, New Zealand, in 1984, and the Ph.D. degree in electric engineering from The University of Queensland, Australia, in 1990. He has been an Associate Professor of electrical engineering at the Auckland University of Technology (AUT), since 1994. Before joining AUT, he was on the Faculty at Karlstad University, Sweden, following a position at the Swiss Federal Institute of Technology (ETH), Zürich, Switzerland. He is currently the Director of the Research-Based Industrial Information and Control Centre (I2C2). His main research interests include modeling, simulation, and control of industrial processes.

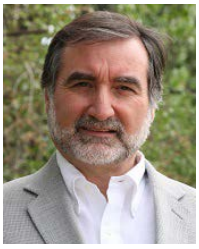

JOSÉ R. PÉREZ-CORREA received the M.Eng. degree in chemical engineering from the Universidad de Chile, in 1982, and the Ph.D. degree in chemical engineering from Imperial College London, in 1987. Since 2011, he has been a Full Professor at the Chemical and Bioprocess Engineering Department, Pontificia Universidad Católica de Chile (PUC). He is currently the Head of the Chemical and Bioprocess Department, PUC. His research interests include dynamic modeling, optimization, and automatic control of chemical processes and bioprocesses.